Received: 28 March 2022 | Revised: 4 May 2023 | Accepted: 12 June 2023

DOI: 10.1002/eqe.3955

RESEARCH ARTICLE

WILEY

Direct loss-based seismic design of reinforced concrete frame and wall structures

Roberto Gentile[1] | **Gian Michele Calvi**[2]

[1]Institute for Risk and Disaster Reduction (IRDR), University College London, London, UK

[2]Scuola Universitaria Superiore IUSS, Pavia, Italy

Correspondence
Roberto Gentile, Institute for Risk and Disaster Reduction, University College London, London, UK.
Email: r.gentile@ucl.ac.uk

Funding information
H2020 Marie Skłodowska-Curie Actions

Abstract

This paper presents a procedure to design reinforced concrete (RC) buildings to achieve an acceptable target level of earthquake-induced loss (e.g., deaths, dollars, downtime) under a site-specific hazard profile. The procedure is called "direct" since the target loss level is specified at the first step of the process, and virtually no iteration is required. The procedure is based on a simplified loss assessment involving a surrogate model for the seismic demand (i.e., probability distribution of peak horizontal deformation given ground-motion intensity) and simplified loss models for direct and indirect losses. For an arbitrarily-selected target loss level and structural geometry, the procedure provides the force-displacement curve of the corresponding equivalent single degree of freedom system. The principles of displacement-based design are adopted to provide member detailings (beams, columns, walls) consistent with such force-displacement curve. The procedure is applied to 16 realistic RC case studies with a lateral resisting system composed of frames in one direction and cantilever walls in the perpendicular one. They show different geometries, hazard profiles, and target values of direct economic expected annual loss. A benchmark loss estimation is obtained using cloud-based non-linear time-history analyses of multi-degree of freedom models. The procedure is conservative since the benchmark loss levels are always smaller than the targets. Such discrepancy is within 10% for 12 out of 32 case studies, between 10% and 20% for 13, between 20% and 31% for the remaining six. Therefore, the proposed procedure is deemed dependable for preliminary design.

KEYWORDS
displacement based design, earthquake risk, non-linear time history, seismic design

1 | INTRODUCTION AND MOTIVATION

Provisions in seismic design codes generally focus on collapse prevention or life safety for major, rare earthquakes while damage prevention for minor, frequent ones. The evolution of theoretical knowledge, modelling abilities, and actual dam-

NOVELTY

- A direct loss-based seismic design (DLBD) procedure is proposed
- The target loss level is specified at the first step of the process
- Virtually no design iteration is required; usually two or three are sufficient
- DLBD is applied to 32 realistic reinforced concrete case studies: 16 frames and 16 cantilever walls
- Validation is conducted against a refined loss assessment based on non-linear time-history analyses

age observations led to higher awareness of the implications of code provisions on earthquake risk (e.g., ref. [1]). The devastating economic consequences of the 1994 Northridge (USA) event symbolically marked the need for a paradigm shift in evaluating the performance of structures to consider the implied effects on society. Extensive research efforts led to the introduction of performance-based earthquake engineering (PBEE[2]), which was later codified in a fully-probabilistic earthquake loss assessment approach[3], now considered a standard (sometimes called "the PBEE formula").

For a given structure, the PBEE formula allows deriving the mean annual frequency of exceeding a decision variable (e.g., casualties/injuries, economic loss, downtime) by integrating: (1) a hazard curve, representing the frequency of exceeding different values of a ground motion intensity measure (IM) for a given site; (2) a fragility model, representing the probability of a structure to reach/exceed different structure-specific damage states (DSs), depending on specific engineering demand parameters (EDP), often related to deformation, and (3) a damage-to-loss model, representing the probability distribution of the selected decision variable (e.g., economic loss) as a function of the selected DSs. Each PBEE module can be characterised for the entire structure (global-level approaches, e.g., ref. [4]), or in a component-by-component fashion (e.g., refs. [5, 6]). The latter approach is likely to return more-refined results, although it requires a more detailed input. The loss assessment procedure described in Section 2 pertains to the global-level category.

Starting from force-based design (e.g., ref. [7]), different research efforts included risk-related concepts within the seismic design process. This involves defining a structure (considering structural and non-structural components) that complies with a given target decision variable (different than a base shear). Such a procedure may involve some or all the loss assessment modules, and this is reflected in the adopted decision variable. A non-exhaustive list of examples may include procedures targeting displacement as a decision variable, such as direct displacement-based design[8] or yield point spectra[9]; methods targeting seismic fragility (e.g., refs. [10, 11]), both used for new design or retrofit; procedures targeting the mean annual frequency of exceeding a given DS, such as the yield frequency spectra approach[12], the probabilistic displacement-based design[13,14], or the risk-targeted force-based design[15]; procedures targeting losses, discussed in more details below; resilience-based methods[16]. A review of different possible performance-based design approaches is given in refs. [17] and [18].

Most of the available risk-related design procedures are iterative since loss assessment is a highly non-linear mathematical problem considering, among many other factors, that the fragility module depends on non-linear time-history analyses (NLTHA). Therefore, such procedures involve repeated applications of an assessment formula while revising a guess design candidate until the target decision variable is met. Although this allows fine-tuning each structural or non-structural component of the design candidate, it tends to be particularly demanding in computational effort and time. Such approaches are arguably more appropriate for the advanced design stages than the conceptual or preliminary design phases. Direct procedures, arguably more suitable for preliminary design, require an explicit mathematical formulation (e.g., mapping a decision variable to the structural and non-structural parameters). Given the complexity of the loss-assessment problem, this can be efficiently achieved only by accepting a trade-off between the simplicity of the adopted framework and the refinement of the solution (e.g., ref. [19]). For example, this can be achieved by using a global-level rather than a component-by-component assessment, avoiding multi-degree of freedom NLTHA, adopting pre-computed hazard models, etc. The assumptions adopted within this paper are described in Section 2.

It is worth narrowing the scope of this discussion to the loss-based design procedures available in the literature, which mainly focus on direct economic losses. Some approaches involve using non-linear optimisation methods and/or trial-and-error[20–24] to obtain design configurations complying with a given loss level. The methods mentioned above involve many iterations of a component-by-component loss assessment for realisations of structures within a specific asset class (e.g., 4-storey RC office buildings). Not only this process requires extensive computational effort, but it also provides low flexibility to the design process. In particular, this requires assuming the number and typology of non-structural components, most

likely not known in the conceptual and preliminary design phases. Rather than using automated design algorithms, other approaches (e.g., ref. [25]) involve iterative design considering guidelines for structural adjustment aimed at increasing strength and/or system ductility, and involve computing risk using increasingly refined analysis methods (e.g., linear analysis, pushover, NLTHA).

Other approaches are based on pre-computing the PBEE formula for many structural configurations within a class. For example, the preliminary PBEE approach[26], also in line with the conceptual guidance in ref. [24], provides the means to derive design charts mapping the desired loss level (for a given IM level) to a given structural period. Such charts refer to one specific structural class, and they are obtained through a component-by-component loss estimation for all the possible structural configurations within the class. Therefore, this approach is affected by the two limitations mentioned above.

The procedure in ref. [27] involves a global-level loss assessment pre-computed for a set of single degree of freedom (SDoF) systems, allowing to define a set of equivalent seismic loss spectra (ultimate displacement vs. base shear for a given value of loss). This procedure allows for comparing different SDoF systems during the preliminary design phase. Although this procedure seems somehow appropriate for the preliminary design phase, it suffers from some drawbacks such as: (1) it does not directly link a design candidate to a target loss (it only allows comparing different systems); (2) it requires running NLTHAs of a large set of SDoF systems for each new design; (3) it does not adopt state-of-the-practice fragility/vulnerability models; (4) it does not allow considering indirect losses (e.g., cost of relocation during repairs); (5) it only allows a hazard model dependent on peak ground velocity and (6) it does not provide a structural detailing phase (i.e., it only involves SDoF systems).

This paper presents a direct loss-based design (DLBD) procedure for reinforced concrete (RC) frame and wall lateral resisting systems overcoming the above limitations. DLBD aims at designing structures that would achieve, rather than be bounded by, a given loss-related metric under the relevant site-specific seismic hazard (by analogy with the words of Priestley[8]). The adjective "direct" refers to the ability of the designer to specify a target loss as an input parameter before running any analysis and to reasonably achieve such a target with few design iterations (e.g., two or three). DLBD was initially proposed by Gentile and Galasso[28], and it is consistent with the conceptual guidance in Calvi et al[29].

The proposed DLBD adopts a global- or storey-level loss-assessment procedure (Section 2) to provide a flexible mapping of different structural and non-structural configurations to the related loss curve (indicating the mean annual frequency of exceeding different loss values). The hazard module is based on hazard curves expressed in terms of spectral acceleration at different fundamental periods of vibration. This feature allows exploiting hazard models available for many world regions (e.g., ref. [30]) to obtain a site-specific hazard mapping with no effort. The fragility module is based on metamodels using Gaussian process regression (developed in ref. [28]), therefore not requiring any NLTHA (similarly to other methods, such as ref. [31]). Such metamodels map the parameters that control the dynamic behaviour of inelastic SDoF systems (e.g., force-displacement capacity curve, hysteretic behaviour) to their probabilistic seismic demand model (PSDM; i.e., conditional probability distribution of an EDP given an IM). PSDMs immediately lead to building-level fragility curves for a selected set of structure-specific damage states. Direct losses are based on building- or storey-level loss models (described in Section 2), thus allowing flexibility in choosing the loss type (e.g., casualties, economic losses, downtime). Apart from using a consequence model, indirect losses (e.g., cost of relocation during repairs) can also be included using a recently-proposed non-linear map to direct ones to be calibrated according to the selected indirect loss type.[29]

The result is a flexible and fast loss mapping returning the force-displacement curve of a candidate design SDoF complying with the desired target loss. This allows to effectively decouple the (somehow automatised) high-level identification of an ideal system complying with a target loss, to the (traditional) low-level detailing process, which is much more common in the practice than the previous step. At this stage, any structural-detailing procedure could be adopted to design each member of the system to comply with the target force-displacement curve. Herein, direct displacement-based design principles are suggested and described for both RC frame and wall lateral resisting systems.

From a computational point of view, calculating a loss mapping may be similar to the loss calculation for different SDoF systems within an iterative non-linear optimisation algorithm. However, the design experience of the user in the two cases above is fundamentally different. Using an optimisation algorithm, the designer can only set an objective function to minimise, and then accept the final result of the optimisation. With DLBD, a conceptual design phase is possible (Section 3.4): the designer is allowed to critically think about their choices (e.g., lateral resisting system, force/displacement capacity) against the implications in terms of loss, which are not always trivial to anticipate based on experience due to the high non-linearity of the loss estimation problem.

After discussing the adopted simplified earthquake loss analysis procedure (Section 2), this paper describes the proposed direct loss-based design (Section 3). The procedure is used to design 32 RC frame and wall lateral resisting systems, and

the results are validated against NLTHA-based refined loss estimations using multi degree of freedom (MDoF) structural models (Section 4). Finally, conclusions are drawn in Section 5, together with further research needs.

2 | SIMPLIFIED EARTHQUAKE LOSS ASSESSMENT

2.1 | Surrogated probabilistic seismic demand model

The PSDM adopted in this paper is the bi-linear model in Equation (1). It allows calculating the distribution of ductility demand μ (i.e., the selected EDP) conditioned on the intensity measure $R = SA/f_y$, where SA is the pseudo-spectral acceleration at the elastic period of the SDoF (in the units of [g]) and f_y is its yield strength normalised by its weight. The behaviour in the elastic range follows from the definition of an elastic SDoF, and it is deterministic. The inelastic range, for which the median prediction is $\mu = a(R-1)+1$, is defined by two parameters: the slope a, and the logarithmic standard deviation, σ, of the pairs $\mu - 1$ versus $R - 1$. ε is a standard Normal variable. This model implies homoscedasticity for $\mu > 1$ and a Lognormal distribution of the residuals, which is desirable in calculating Lognormal fragility curves. It is worth mentioning that although more advanced IMs are available (e.g., ref. [32]), choosing R may simplify the hazard analysis in practical applications or even allow exploiting existing hazard models. Clearly, the above PSDM does not explicitly consider the mechanical coupling between structural and non-structural components.

$$\begin{cases} \mu = R & \mu \le 1 \\ \ln(\mu - 1) = \ln(a) + \ln(R-1) + \varepsilon\sigma & \mu > 1 \end{cases} \tag{1}$$

A crucial component of the simplified loss assessment at the basis of the proposed DLBD procedure is the direct calculation of the parameters (a, σ) using the surrogate PSDM proposed by Gentile and Galasso[28]. This allows analytical estimations of seismic demand, substituting multiple NLTHAs with the direct, computationally-cheap estimations of the parameters of the PSDM (a, σ). Gentile and Galasso define a training dataset of 10′000 inelastic SDoFs, each subjected to a cloud-based NLTHA using 100 natural (i.e., as recorded) ground motions. The SdoFs in the dataset are defined with combinations of the input parameters controlling their inelastic dynamic behaviour up to their peak force capacity (thus covering damage levels up to the so-called "near collapse" DS): fundamental period T, controlling the elastic stiffness; the yield shear strength, normalised to the total weight f_y; the hardening ratio h; the hysteresis model "$hyst$", governing stiffness degradation under unloading-reloading conditions. Five different hysteresis models are currently considered: Kinematic hardening; Modified Takeda "fat"; Modified Takeda "thin"; Modified Sina; Flag shape. The remaining parameters are currently limited to the ranges $T \in (0.2s, 1.5s)$; $f_y \in (0.05, 0.6)$; $h \in (0, 0.3)$. The PSDM in Equation (1) is fitted using the available 100 NLTHA runs for each SDoF in the dataset, thus estimating the parameters (a, σ), which are used as output variables in the training dataset. Finally, a $(hyst, T,\ f_y,\ h)$—(a, σ) mapping is obtained fitting two Gaussian process regressions[33] to the above input-output dataset, thus allowing analytical, computationally-cheap estimations of the PSDM parameters (a, σ), given the SDoF input parameters $(hyst, T,\ f_y,\ h)$. GP regressions are adopted since they do not require any a priori definition of the output functional form (they are non-parametric models), and they ensure high accuracy and flexibility in earthquake engineering applications (e.g., ref. [34]). A 10-fold cross validation is used to test the above GP regressions in predicting the parameters (a, σ) of the SDoF database, respectively, recording a normalised root mean squared error of 2.6% and 6.3%. Moreover, the results are benchmarked against refined NLTHA of eight realistic RC frames (i.e., non-linear, component-by-component MDoF models), recording errors in the range 17%−24% in estimating the median of fragility functions for four DSs. More details on the fitting procedure, the fine-tuning of the models, and the adopted datasets are given in ref. [28], while the code implementation is freely available (https://github.com/robgen/surrogatedPSDM). Apart from the functions to predict the parameters (a, σ), the repository includes the adopted training datasets and the code to train the GP regressions so that users can filter, extend, or modify the training dataset and update the fitting.

2.2 | Fragility and loss analysis

For a given SDoF, once the PSDM parameters (a, σ) are evaluated using the $(hyst, T,\ f_y,\ h)$—(a, σ) mapping, it is possible to derive fragility functions to perform seismic risk/loss analysis. Building-level fragility curves are calculated for a set of

structure-specific DSs, identified by the thresholds EDP_{DS}. One possibility involves choosing four DSs: slight, moderate, extensive, and complete damage, as defined according to HAZUS[35]. Including a degree of approximation, those can be considered similar to immediately operational, damage limitation, significant damage (life safety), and near collapse in Eurocode.[36] Other definitions of the DSs are possible[36,37], and the proposed loss assessment procedure is independent of their particular choice.

According to the properties of the adopted PSDM (Equation 1), Lognormal fragility curves for each DS, representing the DSs' exceeding probability are entirely specified by their median η_{DS_i} and logarithmic standard deviation β (simply called dispersion), which are given in Equation (2) both for the elastic and inelastic ranges. Considering the intensity measure R, they are expressed as $F_{DS_i}(R) = P(\mu \geq \mu_{DS_i}|R) = \Phi(\ln(R/\eta_{DS_i})/\beta)$, where Φ is the standard Normal cumulative distribution. More conveniently, they can be represented in the form $F_{DS_i}(SA)$ by multiplying the median η_{DS_i} by f_y and keeping the dispersion unchanged.

$$\mu_{DS_i} \leq 1;\ \begin{cases} \eta_{DS_i} = \mu_{DS_i} \\ \beta = 0 \end{cases} \qquad \mu_{DS_i} > 1;\ \begin{cases} \eta_{DS_i} = \frac{\mu_{DS_i} - 1}{a} + 1 \\ \beta = \sigma \end{cases} \tag{2}$$

If the fragility parameters calculated with Equation (2) are used to represent MDoF structures, $\beta = \sigma$ should be also adopted for the elastic range, as suggested in ref. [28]. This is to account for the variability of structural response (and, in turn, losses) in the elastic range. By adopting a hazard curve appropriate for the considered SA, representing the mean annual frequency of exceeding (MAFE) a given value of SA (λ_{SA}), it is possible to calculate the MAFE related to each DS (λ_{DS}), as a measure of damage-state safety. This is done with Equation (3).

$$\lambda_{DS} = \int_0^{\infty} F_{DS_i}(SA) \times \left| \frac{d\lambda_{SA}}{dSA} \right| dSA \tag{3}$$

2.3 | Loss analysis

2.3.1 | Direct losses

Two alternative methods for loss analysis–involving different refinement levels–are envisioned for DLBD: (1) building-level analysis based on a vulnerability curve collectively representing the structure and the non-structural components (*low refinement*); (2) storey-level analysis based on a vulnerability curve for the structure and storey loss functions[38] for non-structural components (*medium refinement*). High-refinement, component-based loss assessment methodologies (e.g., ref. [5]) are not considered since they are deemed appropriate for more refined applications, rather than preliminary/conceptual design (e.g., the detailed seismic loss estimation of strategic buildings). If the designer has enough information to confidently characterise an inventory of non-structural components since the preliminary design phase, the medium-refinement approach may be chosen. Contrarily, a low-refinement method is advisable.

Building-level vulnerability curves for the low-refinement method can be derived using a building-level model mapping consequences to each building DS (structural and non-structural). For example, consequences can involve direct economic losses due to structural or non-structural damage, content damage, or a combination of the two. Other consequence models can involve casualties and injured occupants or business interruption (repair or downtime, loss of income). The consequence levels corresponding to different building DSs are herein generically called damage-to-loss ratios (*DLRs*). HAZUS[35] provides examples of building-level consequence models for the above-mentioned categories Equation (4) defines the expected direct building loss (as a ratio of the total reconstruction cost, LR_D) for a given SA value. It refers to a vulnerability curve (Figure 1A) involving the difference between fragility curves of the $(i+1)^{th}$ and i^{th} DSs (and $F_{DS_0} = 1$).

$$LR_D(SA) = \sum_{i=1}^{4} \left(F_{DS_{i-1}}(SA) - F_{DS_i}(SA) \right) \times DLR_i \tag{4}$$

The alternative, medium-refinement loss-assessment method is herein described considering economic losses. First, a vulnerability curve only related to the structural system (herein named LR_{Str}) is defined. This is done using Equation (4)

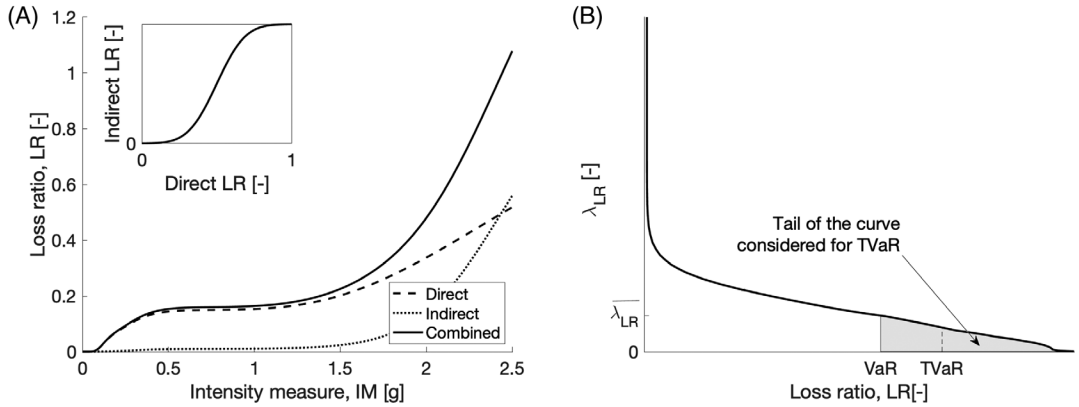

FIGURE 1 (A) Vulnerability curves; (B) Loss metrics defined using the loss curve. $\boldsymbol{\lambda_{LR}}$, mean annual frequency of exceeding a loss ratio; TVaR, tail value at risk; VaR, value at risk.

and a set of DLRs only accounting for structural damage (e.g., ref. [35]) and normalised with respect to the total reconstruction cost of the building. Non-structural components are explicitly considered using storey loss functions.[38] They express the probability distribution of a storey-level consequence variable (e.g., economic loss) of a group of non-structural components versus an appropriate EDP. According to a common assumption, non-structural components are grouped into drift- sensitive and acceleration-sensitive ones. A mean storey loss function may be represented by the five-parameter (p_1 to p_5) regression model in Equation (5), proposed and validated in ref. [39]. Equation (5a) refers to a group of drift-sensitive non-structural components located at storey i, using peak storey drift (θ_i) as an EDP while Equation (5b) uses peak storey acceleration (a_i) for acceleration-sensitive ones. $CF_{NSD,i}$ is a cost factor representing the total value of the drift-sensitive non-structural components at storey i normalised by the total reconstruction cost of the building ($CF_{NSA,i}$ is the analogous cost factor for acceleration-sensitive ones). Different procedures are available to calibrate the parameters p_1 to p_5 for each group of components (e.g., ref. [40]).

$$LR_{NSD,i}(\theta_i) = CF_{NSD,i} \times \left[p_5 \frac{\theta_i^{p_1}}{p_2^{p_1} + \theta_i^{p_1}} + (1 - p_5) \frac{\theta_i^{p_3}}{p_4^{p_3} + \theta_i^{p_3}} \right] \tag{5a}$$

$$LR_{NSA,i}(\alpha_i) = CF_{NSA,i} \times \left[p_5 \frac{\alpha_i^{p_1}}{p_2^{p_1} + \alpha_i^{p_1}} + (1 - p_5) \frac{\alpha_i^{p_3}}{p_4^{p_3} + \alpha_i^{p_3}} \right] \tag{5b}$$

The next step of the medium-refinement method involves expressing Equations (5a, b)–considered as inputs–as a function of SA. To do so for drift-sensitive non-structural components, Equation (1) is first converted in the form $\Delta(SA)$, involving the peak displacement of the SDoF. This is trivially done using f_y and the yield displacement (Δ_y), which is only dependent on the structural geometry (see Equation 12 in Section 3.1). By using an appropriate displacement shape, the relationship $\theta_i(\Delta)$ for each storey is calculated (Section 3.3 describes appropriate displacement shapes for frames, Equation 14, and for walls, Equation 19). After defining the $\theta_i(SA)$ relationship, it is possible to define the required $LR_{NSD,i}(SA)$ for each storey.

The $LR_{NSA,i}(SA)$ mapping is obtained starting from Equation 6[5]), where H is the total building height, H_i is the height of storey i from the ground, and $S = \max(1, R)$. The parameters a_0 to a_5, calibrated for frames or for walls, are provided in ref. [5]. The hazard curves defined for SA and PGA allow defining the relationship $PGA(SA)$, so that the mapping $\alpha_i(SA)$ is completed, and $LR_{NSA,i}(SA)$ is derived. The vulnerability curve of the building, considering direct losses only, is finally obtained with Equation (7) (i.e., the medium-refinement alternative to Equation 4).

$$\alpha_i(PGA) = \exp\left(a_0 + a_1 T + a_2 S + a_3 \frac{H_i}{H} + a_4 \left(\frac{H_i}{H}\right)^2 + a_5 \left(\frac{H_i}{H}\right)^3 \right) \times PGA \tag{6}$$

$$LR_D(SA) = LR_{Str}(SA) + \sum_i LR_{NSD,i}(SA) + \sum_i LR_{NSA,i}(SA) \tag{7}$$

2.3.2 | Indirect losses

Indirect economic losses refer to anything not directly related to building damage: for residential buildings, those may involve the cost of relocating the displaced building occupants during the emergency phase and the time required to repair and refurbish the damaged building. Apart from using damage-to-repair time models (e.g., ref. [35]), one possible way to consider indirect losses is to assume they are non-linearly mapped to direct ones[29]. Indeed, minor damage (and therefore direct loss) would generally not imply any interruption of the regular building activity. Contrarily, for direct loss levels well below the total loss, the downtime could be close to the expected maximum. According to Calvi et al.[29], Equation (8) provides the indirect loss ratio (LR_I), in which $R_{I/D}$ is the ratio of the maximum indirect-to-direct losses and s is a parameter controlling the non-linearity of the dependence (qualitatively similar to the standard deviation in a Normal cumulative distribution). By applying such a mapping to the vulnerability curve for direct losses (Equation 4), one can calculate the vulnerability curve for indirect losses (Figure 1A).

For residential buildings, only considering the cost of relocating residents, Calvi et al.[29] suggest using Equation (8) with $R_{I/D}$ approximately equal to 1 and s within the range [0.06,0.08]. First, such a formula involves a linear mapping of LR_D, defined in the range [0, 1], to the interval [−0.2, 0.2] through the relationship $l\ r_D = -0.2 + 0.4LR_D$. Then, the Normal cumulative distribution function with zero mean and standard deviation s is defined. The result is represented in the LR_I versus LR_D space. The authors of such research highlight that both Equation (8) and the related parameters are reasonable but arbitrary, and validation is still required. The calibration of the methodology in ref. [29] (based on the selected source of indirect losses to consider in the design), is outside the scope of the present paper. This simplified methodology to estimate indirect losses is herein included to highlight the ability of the proposed design procedure to account for indirect losses explicitly (such that they can be included when more-refined calibrations become available).

$$LR_I = R_{I/D}\,\Phi\left(\frac{lr_D}{s}\right) = \frac{R_{I/D}}{s\sqrt{2\pi}}\int_0^{lr_D} e^{-\frac{lr_D^2}{2s^2}}\,dlr_D \tag{8}$$

2.3.3 | Loss metrics

By matching the hazard frequency of exceeding (λ_{IM}) to the correspondent loss ratios on the vulnerability curve (for direct, indirect or combined losses), it is possible to define the loss curve (Figure 1B), representing the mean annual frequency of exceeding a given loss level (λ_{LR}). The simplest possible loss metric to be used in loss-based design is the value at risk (VaR, Equation 9, Figure 1B), defined as the loss corresponding to a selected mean annual frequency of exceeding $\overline{\lambda_{LR}}$ (or, equivalently, to a given IM). Such value can also be defined based on a selected confidence level[41], which is a proxy for the level of risk aversion of the decision maker (e.g., the building owner). To consider loss levels corresponding to different exceeding frequencies, while keeping the ability to consider risk aversion, one could adopt the tail value at risk ($TVaR$, Equation 10, Figure 1B). This corresponds to the area under the right tail of the loss curve (i.e., the expected value of LR, given that LR is greater than the selected VaR). Finally, one of the loss metrics most commonly adopted in practice is the expected annual loss (EAL). This is equal to $TVaR$ corresponding to $VaR = 0$, and it can also be calculated directly using the vulnerability and the hazard curves (Equation 11).

$$VaR = LR\left(\overline{\lambda_{LR}}\right) \tag{9}$$

$$TVaR = \mathbb{E}\left[LR|LR \geq VaR\right] = \int_{VaR}^{+\infty} LR \times \lambda_{LR} dLR \tag{10}$$

$$EAL = TVaR\left(VaR = 0\right) = \int_0^{+\infty} LR\left(IM\right) \times \left|\frac{d\lambda_{IM}}{dIM}\right| dIM \tag{11}$$

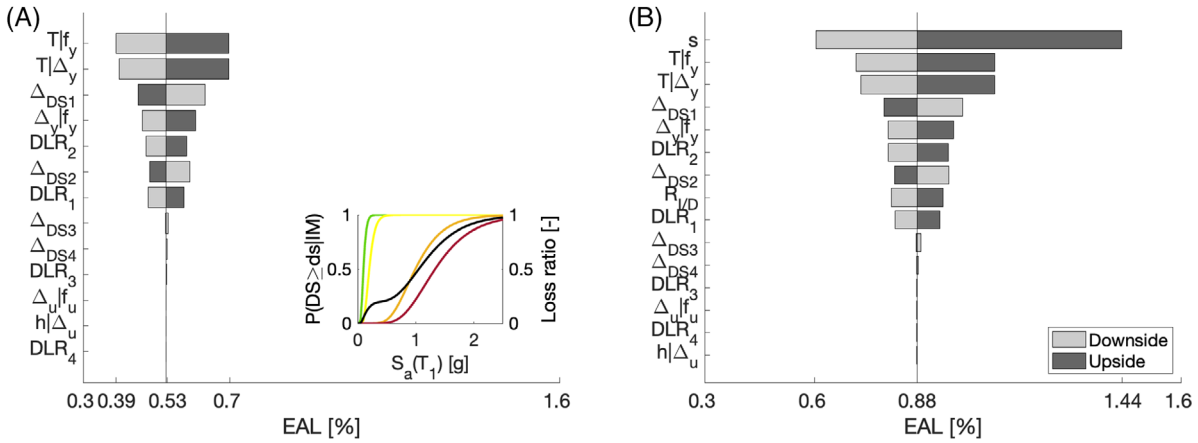

FIGURE 2 Sensitivity of the expected annual loss to different parameters (perturbed by ±20%), neglecting (A) and considering (B) indirect economic losses.

2.4 | Sensitivity analysis

This Section shows the sensitivity of the proposed simplified loss assessment procedure to the main involved parameters. Not only this exercise allowed fine-tuning of the proposed DLBD procedure (Section 3), it also facilitates interpreting any discrepancies between the loss targeted by DLBD and benchmark loss values obtained with more-refined estimation methods (Section 4).

An illustrative (arbitrary) case-study SDoF is selected. It represents a newly-design RC frame building, and it shows a secant-to-yielding period equal to 1s, a weight-normalised yield strength equal to 0.2, a hardening ratio equal to 0.02, and a "Fat" Modified Takeda hysteresis. The system is characterised according to the four above-mentioned structure-specific DSs qualitatively defined according to HAZUS. Those are quantitatively measured on the SDoF backbone, resulting in the displacement thresholds $\Delta_{DS1} = 0.025m$, $\Delta_{DS2} = 0.05m$, $\Delta_{DS3} = 0.225m$, $\Delta_{DS4} = 0.3m$, respectively, for slight, moderate, extensive and complete damage. The median of the fragilities is equal to 0.1g, 0.2g, 0.99g and 1.33g for DS1, DS2, DS3 and DS4, respectively. The dispersion of DS4 is equal to 0.37, and it is adopted for all DSs, as suggested and motivated in ref[28]. Figure 2(A) shows the fragility and vulnerability curves for this base-case SDoF. Consistently with the assumptions in ref. [42] for residential buildings, DLRs equal to 10%, 20%, 50% and 100% of the total reconstruction cost (DS1 to DS4) are assumed. Finally, a hazard curve appropriate for a high-seismicity site in Italy (L'Aquila) is adopted[30]. Section 4 provides details on the adopted model. Considering direct losses only, the EAL of the base-case SDoF is equal to 0.53%. If indirect losses (only considering the cost of relocating residents) are considered according to Equation (8), assuming $R_{I/D} = 1$ and $s = 0.08$, the EAL increases to 0.88%.

A sensitivity analysis on the EAL is carried out by perturbating N input parameters: period T (conserving the yield displacement Δ_y and re-calculating f_y); hardening ratio h (conserving the ultimate displacement Δ_u and re-calculating the ultimate strength f_u); Δ_y (conserving f_y and re-calculating T); Δ_u (conserving Δ_u and re-calculating h); Δ_{DS_i} for each DS; DLR_i for each DS. Each input parameter is increased or decreased by ±20% to define upper and lower bounds. $2N$ perturbations of the above loss analysis are conducted by using one perturbated parameter and the base-case value for the remaining parameters. The sub-set of perturbations in which an input parameter is increased (decreased) is named *upside* (*downside*). The results are shown in a tornado plot (Figure 2), where the horizontal axis represents the EAL (a vertical line is drawn to represent the base-case EAL). The input parameters are listed on the vertical axis. For each perturbation, a horizontal line represents the change in EAL with respect to the base case. The sensitivity of EAL to each input parameter is measured by combining the upside and downside bars. The input parameters are ordered top-to-bottom for decreasing values of the sensitivity. The outcome of this procedure visually resembles a tornado[43].

By neglecting indirect economic losses in the tornado analysis (Figure 2A), the most influential parameter is the fundamental period. If increased by 20%, EAL becomes 30% higher than the base-case value (if decreased, EAL becomes 28% lower). Considering the specific base-case period value, an increase in $T|\Delta_y$ leads to a slightly less-severe hazard curve and a comparatively higher effect on the PSDM (due to the reduced stiffness). Thus, the overall result is an increase in EAL. Although an increase in $T|f_y$ has the same effect on the hazard curve and the PSDM, the EAL is slightly different because a change in Δ_y also involves a change in the DS2 threshold (which is generally related to Δ_y). This tornado

analysis also highlights the importance of the slight damage state (DS1). Indeed, the DS1 threshold and the related damage to loss ratio are the third and fifth parameters if ranked according to their sensitivity on the EAL (a similar effect is seen with Δ_y, perturbated conserving the yield strength). The effect of these parameters provides changes in the vulnerability curve within a ground motion intensity range characterised by high frequency (according to the hazard curve). Clearly, according to Equation (11), this has a high impact on the final loss estimation. Contrarily, parameters related to the extensive and complete damage states produce a minor sensitivity to EAL, as easily inferred from Equation (11).

Figure 2(B) shows the results of a tornado analysis which includes indirect losses. Such analysis highlights the importance of considering indirect losses using a sufficiently-accurate model since when they are considered they cause the highest impact on the results. In particular, however, a 20% increase (decrease) of the ratio of the maximum direct-to-indirect losses only generates an 8% relative increase (10% relative decrease) of the EAL. On the other hand, the parameter s, controlling the shape of the direct-versus-indirect loss curve, is the most influential parameter, causing the EAL to be approximately doubled or halved when it is, respectively, increased or decreased by 20%. Although $R_{I/D}$ may vary in the range[1,5] for different structural typologies,[29] these results qualitatively show that, for practical purposes, a simplified-yet-reasonable estimation of such parameter is sufficient. On the other hand, a more refined estimate of s is paramount for accurate loss estimation and effective design using DLBD. Further research is required to provide reliable estimates of this last parameter.

3 | DIRECT LOSS-BASED DESIGN (DLBD)

The procedure outlined in this Section applies, at this stage, to single frames or walls. Therefore, it can be used for structurally-symmetric buildings composed of parallel frames and walls, analysed in a single plan direction (no torsional effects are considered yet). For this reason, it is conservatively suggested to provide an independent DLBD for each building direction, assuming the same loss target. The code to apply the proposed procedure is freely available in an online repository (https://github.com/robgen/lossBasedDesign).

3.1 | Preparatory steps

Before performing the core of the procedure, it is required to set some assumptions and provide basic input data. With no particular order, the preparatory steps are outlined as follows:

- Provide an appropriate set of site-specific hazard curves in terms of SA in a wide range of periods (or, equivalently, uniform hazard spectra for different return periods), since the period is unknown as it is an intermediate design parameter. The selected hazard curves should reasonably cover the expected range of secant-to-yielding periods of the selected structural typology (e.g., ref. [44]);
- Select a set of DSs (e.g., DS1-DS4 as defined in Section 2.2) relevant to the considered structural typology (e.g., RC frames). Relatively to the unknown ductility capacity at peak strength μ_{cap} (an intermediate design parameter), select reasonable guesses for the DS thresholds consistent with the qualitative definition of the DSs (e.g., $\mu_{DSi} = [0.5,\ 1,\ 0.75\mu_{cap},\ \mu_{cap}]$ may be consistent with the DS definition above). The main aim is to provide μ_{DSi} values as close as possible to those obtainable from the numerical pushover analysis of the final design case;
- Select the typology of losses to consider and a relevant loss metric (e.g., EAL of the direct economic losses from damage to structural/non-structural components and contents);
- Select a relevant damage-to-loss model consistent with the considered loss typologies, the involved structural material and lateral resisting system, and the adopted DSs. For instance, $DL\ R_i = [7,\ 15,\ 50,\ 100]\%$ of the total reconstruction cost are appropriate for direct economic losses of RC buildings[45]. Select an appropriate characterisation of indirect losses (e.g., a direct-to-indirect loss mapping with parameters $R_{I/D}$ and s). If the medium-refinement loss assessment is adopted, select relevant storey loss functions for acceleration- and drift-sensitive non-structural components;
- Select the basic geometric properties of the considered structure, also according to design for other loads (e.g., gravity). Some of these parameters are general, such as the number of storeys (N_{storey}), the inter-storey height (H_{int}), the storey mass M_i, the number of lateral resisting systems resisting in parallel ($N_{parallel}$, allowing to derive the storey mass $m_i = M_i/N_{parallel}$ directly affecting each of them). Some other geometrical parameters depend on the selected lateral resisting

system (and the selected structural detailing design method): for RC frames, those involve the number of bays (N_{bay}), the centre-to-centre length of the beams l_b, the depth of beams and columns (h_b, h_c); for RC walls, those involve the length of the wall (l_w) and the average diameter of the longitudinal bars (ϕ_{bl});

- Exploiting the rules of direct displacement-based design, estimate the structural quantities that can be calculated before any analysis is carried out. Notably, the yield displacement (Δ_y) of concrete structures falls in this category[8].Δ_y for frames is obtained in Equation (12a), where H_i is the height of storey i from the ground and δ_i is the displacement shape ($\delta_{roof} = 1$) assumed according to Priestley et al.[8],ε_{sy} is the still yield stress. On the other hand, Equation (12b) provides Δ_y for walls, where h_w is the wall height, and ε_{sy} is the steel yield strain. A relevant parameter within this category for steel structures (not discussed here) may be the elastic stiffness.

$$\begin{aligned} &\text{a) } \Delta_y = \theta_y H_{eff}\,. \quad \textit{Where} \quad \theta_y = \frac{0.5\varepsilon_{sy}(l_b - h_c)}{h_b} \quad \text{and} \quad H_{eff} = \frac{\sum_i m_i \delta_i H_i}{\sum_i m_i \delta_i} \\ &\text{b) } \Delta_y = \frac{\sum \mathrm{m_i}\Delta_{y,i}^2}{\sum m_i \Delta_{y,i}}\,. \quad \textit{Where} \quad \Delta_{y,i} = \frac{\chi_y}{2} H_i \left(1 - \frac{H_i}{3h_w}\right) \quad \text{and} \quad \chi_y = 2\frac{\varepsilon_{sy}}{l_w} \end{aligned} \tag{12}$$

3.2 | Core steps

The core of the procedure allows deriving the capacity curve (displacement vs. spectral acceleration) of the design SDoF. It applies regardless of the selected lateral resisting system, and it is outlined as follows:

- Select a loss target L_{target} (e.g., EAL equal to 0.2% of the total reconstruction cost);
- Select a number of *seed SDoF systems* by defining combinations of the GP regression inputs. The most general case involves defining an arbitrary grid-based design of experiment using all the GP regression inputs (i.e., $hyst, T, f_y, h$), plus the seed ductility capacity μ_{cap}. The range for such parameters should be large enough to ensure including possible design cases. However, engineering judgement may allow avoiding physically unsound values in the mapping, thus also increasing the speed of the calculations. Depending on the considered material and lateral resisting system, some of the above parameters may be considered invariant, thus simplifying the set of seed SDoFs. For RC structures, the most suitable hysteresis type may be set (e.g., MTf for newly-designed frames, MTt for walls). The same applies to the hardening ratio, which can be reasonably set to 0.05 for RC frames and 0.02 for RC walls. Moreover, the yield displacement of RC structures only depends on geometry, and it can be defined in the preparatory steps (Equation 12). Therefore, the yield strength ($f_{y,seed}$) is linearly related to stiffness, and the elastic period of each seed SDoF (T_{seed}) is equal to $T_{seed} = 2\pi\sqrt{\Delta_y/9.81 f_{y,seed}}$. With these assumptions, the set of seed SDoFs can be defined by N_1 equally-spaced points within $f_{y,min}$ and $f_{y,max}$ and N_2 equally-spaced points between $\mu_{cap,min}$ and $\mu_{cap,max}$, leading to $N_1 N_2$ combinations. As mentioned above, the range and spacing of such points should be based on engineering judgement;
- Using the surrogate PSDM, calculate fragility curves for each seed SDoF consistent with the selected DS thresholds μ_{DSi}. As suggested and motivated in ref. [28], adopt the calculated dispersion (σ, Equation 2) both for the elastic and inelastic range. According to the selected refinement level for the loss assessment module, calculate the building-level vulnerability curve for each seed. Using the hazard curve (interpolated based on T_{seed}), calculate the and the EAL for each seed (see Figure 3A);
- Select all the SDoF seeds that meet the target EAL level within a set tolerance (e.g., $EA\ L_{tol} = 0.01 EAL_{target}$). Clearly, the finer the seed-SDoF grid is, the smaller such tolerance can be. For each selected seed, run the capacity spectrum method (CSM[46]) using spectra for each DS demand (code-based, as per Figure 3B, or site-specific ones) and disregard the cases not meeting the code-based seismic demand for any DS (i.e., $\mu_{dem,DSi} > \mu_{DSi}$). In addition, calculate the frequency of exceeding the complete damage DS, by integrating the complete damage fragility with λ_{IM}, analogously to Equation (11), and disregard the cases above a conventionally-established threshold (e.g., between 10^{-5} and 10^{-4}[47]). The seed SDoFs meeting the target EAL, the complete-damage reliability bound, and complying with the code-based displacement check are equally valid *candidate design SDoFs*. Conceptually following the guidelines in ref. [25], the EAL estimation of the candidates can be optionally refined using pushover-based methods (e.g., using ref. [48], which would also allow using a user-defined set of ground motions). One of the candidate design SDoFs can be arbitrarily selected as the final *design SDoF*, possibly according to design requirements not related to seismic actions. This allows the designer meeting the loss target while being granted flexibility to meet non-seismic design constraints.

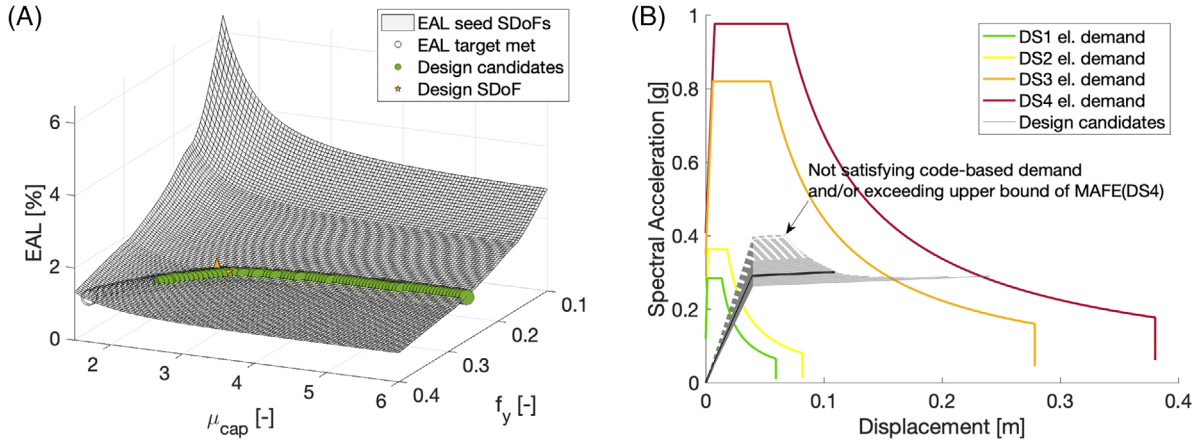

FIGURE 3 (A) Expected annual loss of the seed SDoFs; (B) capacity curves of the candidate design SDoFs. DS, damage state; MAFE, mean annual frequency of exceedance.

3.3 | Structural detailing

Once the design SDoF is determined, one should design each structural member in the lateral resisting system such that the considered structure complies with the design SDoF's backbone. Generally, one must also ensure the structure achieves a favourable plastic mechanism. This process, herein referred to as structural detailing, is not strictly part of the proposed DLBD. In other words, one can adopt any design and analysis method (including trial and error) to achieve this goal. This is possible because DLBD allowed decoupling the process of matching a target loss with a target force-displacement backbone (less common in the practice) to the process of matching a detailing configuration to a target backbone (fairly common in the practice).

For completeness, this Section suggests using the principles of displacement-based design to provide the target strength and deformation capacity of structural members to be used as for detailing. This is done considering symmetric structures -not prone to torsional effects- either composed of RC frames or walls.

3.3.1 | RC frames

The favourable plastic mechanism for RC frames involves plastic hinges for the base column sections and all beams' end sections. For a geometrically-regular RC frame, the beams' plastic drift demand ($\theta_{bi,p}$) compatible with the displacement capacity at peak force (Δ_{cap}) of the design SDoF is calculated according to Equations (13) and (14), where θ_i is the inter-storey drift profile compatible with the displacement profile Δ_i. On the other hand, the drift demand on the first-storey columns (θ_c) is simply equal to the inter-storey drift at that level.

$$\theta_{bi,p} = \theta_{i,p} / (1 - h_c/l_b). \text{ Where } \theta_{i,p} = \theta_i - \theta_y \tag{13}$$

$$\Delta_i = \frac{\Delta_{cap}}{\delta_{eff}} \delta_i. \text{ Where } \delta_{eff} = \frac{\sum_i m_i \delta_i^2}{\sum_i m_i \delta_i} \tag{14}$$

The strength demand for the members developing inelastic behaviour is computed via an equilibrium approach. For RC frames, this involves the overturning moment (OTM) equilibrium[8], according to Equation (15), where $V_B(\Delta_{cap}) = f_{peak} m_{eff}$ is the SDoF base shear, $m_{eff} = \frac{\sum_i m_i \Delta_i}{\Delta_{cap}}$ is the effective mass, $M_{c,k}$ is the base moment of column k, L_{build} is the frame length, $V_{b,ij}$ is the shear of the beam at storey i and bay j. Any allocation of strength to the members developing inelastic behaviour that complies with Equation (11) would satisfy the design objective. One possible design choice may involve assuming (Equation 16) that the contra-flexure point of the first-storey columns locates at 60% of their height so that the capacity design of the first-storey beam-column joints is ensured. Moreover, if the beams have the same detailing in both end sections and within the frame, Equation (17) holds, where $M_{b,ij}(\theta_{bi,p})$ is the beam moment demand corresponding to its plastic drift demand. With such assumptions, it is possible to invert Equation (15) and calculate the beams'

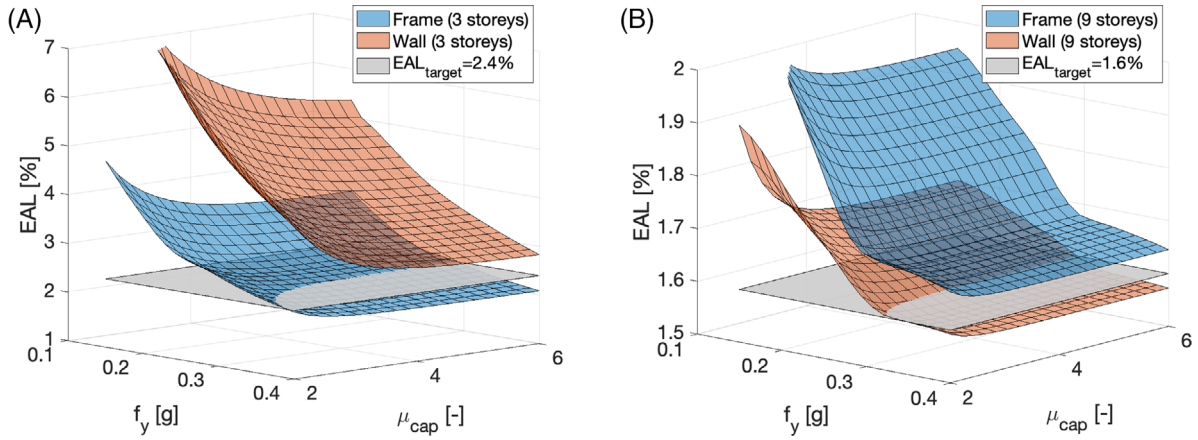

FIGURE 4 RC frame versus wall conceptual design using direct + indirect loss mapping: (A) 3-storey (2% target EAL); (B) 9-storey (1.4% target EAL). Assumptions: hardening $\mathbf{h} = 0.05$; hysteresis "Mod. Takeda fat" for frames, "Mod. Takeda thin" for walls; hazard conditions for L'Aquila, Italy[30]; damage state definition $\boldsymbol{\mu}_{\mathbf{DSi}} = [0.5\ 1\ 0.75\boldsymbol{\mu}_{\mathbf{cap}}\ \boldsymbol{\mu}_{\mathbf{cap}}]$; damage-to-loss ratios $\mathbf{DLR}_{\mathbf{DSi}} = [7\ 15\ 50\ 100]$ %; direct-to-indirect loss characterization $\mathbf{R}_{\mathbf{I/D}} = 2$, $\mathbf{s} = 0.09$; $\mathbf{f_c} = 25\mathbf{MPa}$; $\mathbf{f_y} = 300\mathbf{MPa}$; $\mathbf{l_b} = 6\mathbf{m}$; $\mathbf{N_{bays}} = 4$; $\mathbf{l_w} = 4\mathbf{m}$.

moment demand $M_{b,ij}$ corresponding to the target base shear $V_B(\Delta_{cap})$. The moment demand of the base columns, at $V_B(\Delta_{cap})$, can be proportioned by considering an arbitrary assumption on the relative strength of each column. For example, they can be proportioned assuming that the interior columns will be approximately twice as strong as the exterior ones, thus $M_{c,ext} = 0.6H_1 \frac{V_B(\Delta_{cap})}{2(N_{bay}-1)+2}$ and $M_{c,int} = 2M_{c,ext}$. Alternatively, the moment capacity of all the base columns can be set equal.

$$OTM\left(\Delta_{cap}\right) = V_B\left(\Delta_{cap}\right) \times H_{eff} = \sum_k M_{c,k}\left(\theta_{c,k}\right) + L_{build} \sum_{i,j} V_{b,ij}\left(\theta_{bi,p}\right) \tag{15}$$

$$\sum_k M_{c,k}\left(\theta_{c,k}\right) = \sum_j 0.6H_1 V_{c,k} = 0.6H_1 \times V_B\left(\Delta_{cap}\right) \tag{16}$$

$$V_{b,ij}\left(\theta_{bi,p}\right) = \frac{2M_{b,ij}\left(\theta_{bi,p}\right)}{l_b} \tag{17}$$

Once the theoretical deformation and strength demand of the members developing inelastic behaviour is obtained, the structural details of such members are designed. For an RC frame, this involves the demand for beams $(\theta_{bi,p}; M_{b,ij})$ and first-storey columns $(\theta_{c,k}; M_{c,k})$. The structural details of such members can be designed via a moment-curvature approach. Generally, the provided detailing will lead to a degree of deviation from the theoretical values above. Thus, Equation (15) can be used to re-calculate the peak base shear $V_B(\Delta_{cap})$ provided by the provided design configuration. Moreover, with a reasonable assumption for the hardening (e.g., $h = 0.05$ for RC frames), and by knowing Δ_y, the entire backbone can be calculated and compared to that of the design SDoF (Figure 6A). Such a match is particularly important since it ensures the match between the EAL of the designed frame and the target EAL, at least under the assumptions adopted for the fragility and vulnerability models. Possibly, a pushover analysis can be conducted to further verify the simplified equilibrium/compatibility-based calculations.

Any undesired mismatch between the SDoF and the frame backbone curves may be corrected via: (a) iterations in the member design; (b) revising Δ_y or h, thus restarting from step 2 and (c) based on the results of a pushover analysis, revising the relative definition of μ_{DSi} with respect to the ductility capacity at peak strength μ_{cap}, thus restarting from the preparatory steps. As per any seismic design procedure involving non-linear behaviour, members intended to remain elastic must be capacity protected. Moreover, some member characteristics may be modified to comply with code-based minimum detailing requirements. As demonstrated for seismic failure rates (e.g., ref. [1]), minimum detailing requirements (not necessarily related to seismic provisions) are likely to imply upper bounds of the expected losses for code-conforming buildings, especially in low-seismicity zones. This implies that DLBD is best suited to targeting particularly-low loss values, so that the design is not implicitly controlled by the minimum detailing requirements of the adopted code.

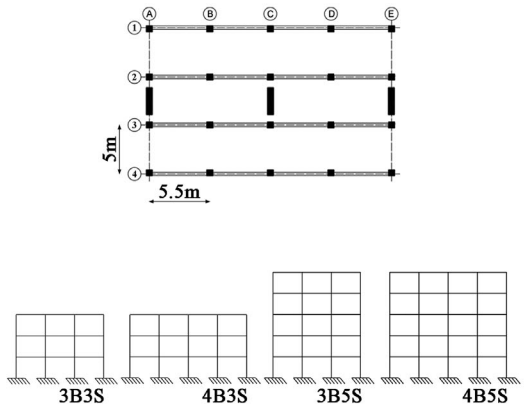

	Nbays	Nstoreys	Seismicity	Target EAL
3B3SAq120EAL	3	3	High (L'Aquila)	1.20%
3B3SAq60EAL	3	3	High	0.60%
3B3SNa120EAL	3	3	Medium (Napoli)	1.20%
3B3SNa60EAL	3	3	Medium	0.60%
3B5SAq50EAL	3	5	High	0.50%
3B5SAq25EAL	3	5	High	0.25%
3B5SNa50EAL	3	5	Medium	0.50%
3B5SNa25EAL	3	5	Medium	0.25%
4B3SAq120EAL	4	3	High	1.20%
4B3SAq60EAL	4	3	High	0.60%
4B3SNa120EAL	4	3	Medium	1.20%
4B3SNa60EAL	4	3	Medium	0.60%
4B5SAq50EAL	4	5	High	0.50%
4B5SAq25EAL	4	5	High	0.25%
4B5SNa50EAL	4	5	Medium	0.50%
4B5SNa25EAL	4	5	Medium	0.25%

FIGURE 5 Geometry, hazard level and EAL target of the selected case-study frames.

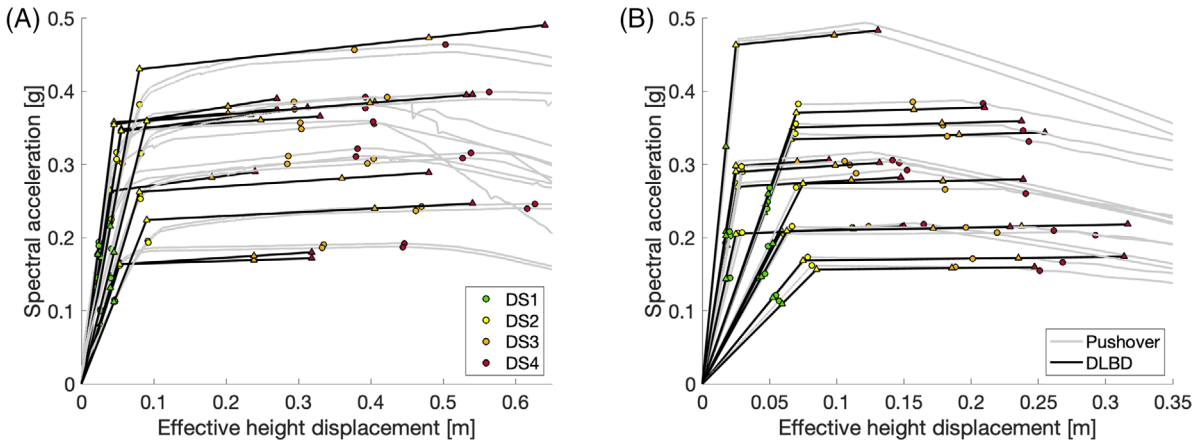

FIGURE 6 Force-displacement curve of the design SDoFs: (A) frame direction; (B) wall direction.

3.3.2 | RC walls

For a system composed of a number of equal RC cantilever walls, each of them is required to form a flexural plastic hinge at the base. Therefore, the main objective of this phase is to determine the target Moment-Curvature relationship of the base section. The curvature at yielding χ_y is available from Equation (12), while the curvature at near collapse χ_{nc} (consistent with Δ_{cap}) is calculated with Equation (18), in which $\chi_{nc,p}$ is the plastic curvature at near collapse, and $\delta_{eff}^{(\chi_p=1)}$ is the effective displacement corresponding to a unit plastic curvature at the base. This last quantity is obtained with Equation (19), in which l_{pl} is the plastic hinge length (calculated conservatively assuming that the effective height is equal to 70% of the total wall height) and f_{sy} is the steel yield stress (which in the context of this formula can be assumed equal to 300 MPa). It is worth repeating that m_i is the storey mass pertaining to one wall.

$$\chi_{nc} = \chi_y + \chi_{nc,p}. \text{ Where } \chi_{nc,p} = \frac{\Delta_{cap} - \Delta_y}{\delta_{eff}^{(\chi_p=1)}} \tag{18}$$

$$\delta_{eff}^{(\chi_p=1)} = \frac{\sum_i m_i \delta_{i,p}^2}{\sum_i m_i \delta_{i,p}} \text{. Where } \delta_{i,p} = l_{pl},\ H_i, \text{ and } l_{pl} = 0.08 * 0.7h_w + 0.1l_w + 0.022 f_{sy}\phi_{bl} \tag{19}$$

The base shear at yielding ($V_{B,y}$) and near collapse ($V_{B,nc}$) is immediately known after calculating the effective mass $m_{eff} = \frac{\sum_i m_i \Delta_i}{\Delta_{cap}}$ substituting the yield (Equation 12b) or near collapse ($\Delta_{nc,i} = \Delta_{y,i} + \chi_{nc,p} l_{pl} H_i$) displacement profiles for Δ_i. Finally, the base moment at yielding and near collapse is obtained with Equation (20), by alternatively substituting $(\Delta_{i,y}, V_{B,y})$ and $(\Delta_{i,nc}, V_{B,nc})$ for (Δ_i, V_B). Via Moment-Curvature analysis, the base section of the wall can be made

consistent with the target curve. As for the frame systems, any mismatch can be corrected via different types of iterations, and capacity protection must be provided.

$$OTM = \sum F_i H_i. \text{ Where } F_i = \begin{cases} 0.9\frac{m_i\Delta_i}{\sum m_i\Delta_i} \text{ for } i = 1, \cdots, N_{storey} - 1 \\ 0.9\frac{m_i\Delta_i}{\sum m_i\Delta_i} + 0.1V_B \text{ for } i = N_{storey} \end{cases} \quad (20)$$

3.4 | Conceptual design considerations

This Section briefly shows the potential of the proposed DLBD in assisting the conceptual phase of the design process by allowing the designer to rationally consider different design options (e.g., different lateral resisting systems) and discriminate among them on the basis of the target loss. The parameters adopted in this Section are indicative. The results should be considered as qualitative.

After applying the DLBD procedure up to step 3, Figure 4 compares the EAL of many seed SDoFs differing only for their considered lateral resisting system (RC frame or wall). In particular, Figure 4(A) refers to a 3-storey building, while Figure 4(B) involves a 9-storey one. Clearly, the frame-versus-wall comparisons are conducted assuming the same values for each parameter required within the preliminary steps of DLBD (those are listed in the caption of the figure). The results show that the frame- and wall-related loss mappings do not intersect, thus clearly indicating that the conceptual design phase may not be affected by the specific choice of yield strength and ductility capacity. Moreover, a frame system is preferable over a wall one for the 3-storey building (Figure 4A) and vice versa for the 9-storey one (Figure 4B). For the 3-storey configuration, some values of the target EAL (e.g., 2.4%) are only achievable with a frame lateral resisting system. Viceversa, no 9-storey frame configurations allow to achieve a 1.6% target EAL. The results of this example may be explained by the values of the yield displacement (Equation 12), which is higher for 3-storey frames than for 3-storey, walls with a 4 m length. As also confirmed by Figure 2(A), the yield displacement is one of the parameters with the highest effect on the EAL, together with the DS1 displacement (which is reasonably proportional to the yield displacement). On the other hand, the yield displacement of 9-storey frames is lower than the one for 4 m-long, 9-storey cantilever walls (assuming an effective height equal to 70% of the total height), thus explaining the opposite result. It is worth restating that the provided example is only qualitative, and that in a more realistic scenario the designer may likely consider a longer wall and/or challenge the cantilever assumption by adopting a dual wall/frame scheme. For any assumed configuration of the lateral resisting system, the designer may add an additional loss mapping to be compared within the conceptual design phase.

Although the provided example may seem particularly simple, it shows the high potential of the proposed DLBD. In fact, provided that the DLBD procedure is specialised for more design cases, the conceptual design approach shown here could be applied considering different materials (e.g., timber, pre-cast concrete, steel) and lateral resisting systems (e.g., dual wall-frame systems, braced frames, rocking structures, base-isolated structures). Further research on this topic is suggested to provide an effective tool for a loss-based conceptual seismic design that is fully customisable with respect to the site-specific hazard conditions, damage state definitions, adopted damage-to-loss models, and considered loss typologies.

4 | VALIDATION AGAINST REALISTIC CASE-STUDY RC FRAMES

4.1 | Description of the case study buildings

The proposed DLBD is demonstrated for 16 concrete rectangular-plan buildings composed of frames in their longitudinal direction and walls in the transverse one (thus considering 32 case-study lateral resisting systems), using the EAL as a loss metric and selecting the low-refinement loss assessment module (an application of DLBD using the medium-refinement loss assessment module is provided in ref. [49]). The results are validated against a more-refined earthquake loss assessment methodology. Such a method is consistent with the one proposed for DLBD (Section 2) although: (1) the building fundamental period is estimated based on the numerical pushover curve (after bi-linearisation), thus affecting the definition of the hazard curve; (2) the DSs are quantified using the member-level results of numerical pushover analyses, consistently with the DS definitions in Section 2.2. Those refer to the first member in the frame reaching the first

cracking, yielding, ¾ of the near-collapse drift and the near-collapse drift, respectively, for DS1-DS4. It is worth mentioning that the member "causing" a given DS may change for different DSs; (3) the response analysis is based on refined NLTHAs of component-by-component MDoF models (instead of the surrogate PSDM of SDoFs). This validation quantifies the loss-estimation error due to assumptions and procedures intrinsically embedded in DLBD, rather than the quality of the calibration of its input parameters. Therefore, this exercise focuses on the estimation of seismic demand (i.e., PSDM) rather than a validation against component-by-component loss estimation methods. If average loss metrics are required, the agreement between building-level and component-by-component loss estimations can be achieved using appropriately calibrated DLRs (as demonstrated in ref. [49]) or, by analogy, appropriately calibrated storey loss functions (e.g., ref. [40]). For the same reason, indirect losses are not considered in this validation since calibration data are not yet available, and their addition would provide a similar error propagation for both the refined and simplified loss assessments. Moreover, a calibration study related to indirect losses is considered out of scope for this paper, which instead aims at showcasing and validating DLBD.

The general details of the buildings are shown in Figure 5. They have four parallel, three- or four-bay, 5 m-spaced frames in the longitudinal direction and two or three walls in the transverse direction (depending on the strength requirements). The buildings can be either located in a high- or medium-seismicity site (herein represented by the cities of L'Aquila and Napoli). The code-based Italian seismic hazard model is adopted[30]. Thus, no ad hoc site-specific probabilistic seismic hazard analysis is explicitly performed. This model provides spectral acceleration values for nine probabilities of exceedance in 50 years. This allows defining hazard curves based on spectral accelerations for 10 natural period values between 0.1s and 2s, assuming rock conditions. The model also characterises epistemic uncertainty by providing difference percentiles of the results. The median of such distribution is adopted herein. The Italian code[50] also provides analytical approximations of the uniform hazard spectra consistent with the above model, including correction factors to obtain, among others, different soil and topography conditions. For this study, a C-type soil category according to the Italian code is assumed (shear wave velocity in the first 30 m within the range 180−360 m/s).

For simplicity, the minimum detailing standards within the Italian seismic code are not explicitly considered. Therefore, regardless of the assumptions described above, the analysed case-study buildings should be considered as ideal, rather than representative of Italian buildings. The target EAL for the case studies, adopted as the design loss metric in both directions, ranges between 0.25% and 1.20% of the total reconstruction cost, and a tolerance equal to $0.01EAL_{target}$ is used. Since the minimum detailing requirements are not considered, the target EAL of some of the case studies can be higher than typical EAL values for newly-built, Italian buildings. The case studies are selected to showcase the proposed methodology, rather than provide loss estimates for Italian buildings.

All buildings share the following input parameters (defined above): $l_b = 5.5m$, $H_{int} = 3.3m$, $h_b = 0.5m$, $h_c = 0.6m$, $\phi_{bl} = 20mm$, $f_c = 30MPa$, $f_{sy} = 450MPa$, $E_s = 200GPa$. The frames are characterised by the MTf hysteresis model, while MTt is used for the walls. The total storey mass is equal to $205Ton$ and $275Ton$, respectively, for the three- or four-bay buildings. Apart from the self-weight of the structure, this is calculated considering a superimposed dead load equal to $3.6KPa$ and a factored live load equal to $0.9KPa$.

The design process involved 10000 seed SDoF systems defined using 100 equally-spaced values of f_y between 0.1 and 0.4 for and 100 equally-spaced μ_{cap} values within 1.5 and 6. Both the damage state definition (including the values of μ_{DSi}) and the DLR_{DSi} exemplified in Section 3.1 are adopted. For each case study, the design SDoF is selected after verifying the compliance against the code-based spectra related to 30, 50, 475 and 975 years mean return periods (using the CSM), and an upper-bound mean annual frequency of exceeding the DS4 damage state equal to 10^{-5}. The structural detailing phase has been conducted according to Section 3.3 both for frames and walls, also using the graphical-user-interface software SLaMAsolver,[51] related to the Simple Lateral Mechanism Analysis (SLaMA[52]). Table 1 shows the resulting structural details for each case study. The effective mass (calculated according to the DDBD principles, as per Section 3.3.1) pertaining to one single frame ranges between 132 and 294Ton (82%–86% of the total mass), while it ranges between 256 and 524Ton for one single wall (76%–85% of the total mass). T_1 ranges between 0.45s and 0.95s for the frame case studies and between 0.61s and 1.13s for the walls. As discussed for the EAL targets, these period values may not be fully representative of Italian buildings, since minimum detailing requirements are herein not considered.

According to the numerical modelling strategy illustrated in Section 4.2, a displacement-control numerical pushover analysis is carried out for each case study using an invariant triangular force profile. Figure 6 compares the resulting capacity curves with the theoretical backbone of the design SDoFs. The comparison is particularly satisfactory since the curves are essentially superimposed for the walls while showing slight discrepancies for the frames' ductility capacity. Figure 6 also compares the DS thresholds used in the simplified loss assessment (triangular marks) against the pushover-based ones used for the refined one (circular marks). For the frames, the displacement-based relative discrepancy ranges

TABLE 1 Structural detailing of the case-study frames.

	Typical beam	Typical column	Walls
3B3SAq120EAL	300 × 450; 2phi14 + 2phi14; phi10@120	400 × 400; 3phi20 + 3phi20; phi10@100	2walls: 200 × 4000; 24phi16; phi10@150′
3B3SAq60EAL	300 × 450; 3phi16 + 3phi16; phi10@120	350 × 350; 3phi18 + 3phi18; phi10@100	2walls: 200 × 4000; 32phi20; phi10@150′
3B3SNa120EAL	300 × 350; 2phi14 + 2phi14; phi10@120	350 × 350; 2phi16 + 2phi16; phi10@100	2walls: 200 × 3500; 20phi16; phi10@150
3B3SNa60EAL	300 × 450; 3phi16 + 3phi16; phi10@120	400 × 400; 3phi16 + 3phi16; phi10@100	2walls: 200 × 3500; 32phi16; phi10@150
3B5SAq50EAL	300 × 500; 3phi18 + 3phi18; phi10@120	400 × 400; 3phi20 + 3phi20; phi10@100	3walls: 200 × 4000; 28phi16; phi10@150
3B5SAq25EAL	300 × 500; 2phi20 + 2phi20; phi10@120	500 × 500; 3phi24 + 3phi24; phi10@100	3walls: 200 × 4000; 38phi20; phi10@150
3B5SNa50EAL	300 × 400; 3phi16 + 3phi16; phi10@120	400 × 400; 3phi20 + 3phi20; phi10@100	2walls: 200 × 3500; 40phi18; phi10@150
3B5SNa25EAL	300 × 500; 2phi20 + 2phi20; phi10@120	450 × 450; 3phi24 + 3phi24; phi10@100	3walls: 200 × 4000; 40phi20; phi10@150
4B3SAq120EAL	300 × 450; 2phi14 + 2phi14; phi10@120	400 × 400; 3phi20 + 3phi20; phi10@100	2walls: 200 × 4000; 32phi18; phi10@150
4B3SAq60EAL	300 × 450; 3phi18 + 3phi18; phi10@120	400 × 400; 3phi16 + 3phi16; phi10@100	3walls: 200 × 4000; 34phi18; phi10@150
4B3SNa120EAL	300 × 350; 2phi14 + 2phi14; phi10@120	350 × 350; 2phi16 + 2phi16; phi10@100	2walls: 200 × 3500; 30phi16; phi10@150
4B3SNa60EAL	300 × 450; 3phi16 + 3phi16; phi10@120	400 × 400; 3phi16 + 3phi16; phi10@100	3walls: 200 × 3500; 28phi16; phi10@150
4B5SAq50EAL	300 × 500; 3phi18 + 3phi18; phi10@120	400 × 400; 3phi20 + 3phi20; phi10@100	3walls: 200 × 4000; 36phi18; phi10@150
4B5SAq25EAL	300 × 500; 2phi20 + 2phi20; phi10@120	500 × 500; 3phi24 + 3phi24; phi10@100	3walls: 200 × 4000; 40phi20; phi10@150
4B5SNa50EAL	300 × 400; 3phi16 + 3phi16; phi10@120	400 × 400; 3phi20 + 3phi20; phi10@100	2walls: 200 × 3500; 44phi20; phi10@150
4B5SNa25EAL	300 × 500; 2phi20 + 2phi20; phi10@120	450 × 450; 3phi24 + 3phi24; phi10@100	3walls: 200 × 4000; 68phi20; phi10@150

All measures are in millimetres.

between −6.7% and 7.2% for DS2 (−6.8% and 9.2%), while −29.5% and 48.1% for DS4 (−15.6% and 29.% for walls). Such discrepancies could have been reduced with more structural detailing iterations. However, considering the expected sensitivity of losses to such thresholds (Section 2.4), discrepancies in the order of the above values are deemed reasonable, and the structural detailing iterations are stopped.

4.2 | Numerical modelling strategy and response analysis method

2D lumped-plasticity models are developed using the finite element software Ruaumoko[53] for each frame and wall configuration, using a modelling strategy extensively validated against experimental results[54]. Floor diaphragms are modelled as rigid in their plane, and fully fixed boundary conditions are considered at the base. P-Delta effects are not modelled since they are deemed negligible for the considered case studies. A 5% tangent stiffness-proportional elastic damping is assigned to all frequencies. The wall members were discretised having an element for each storey. The flexural capacity of the RC members is derived using moment-curvature analysis. The flexural response is checked against other failure mechanisms that may significantly modify the lateral member response. The lateral capacity of the members included in the analysis is modified (if appropriate) to include those failure mechanisms accordingly, considering slab-related flange effect for the negative beam moment capacity, lap splice failure, shear capacity, bar buckling, adopting specific models appropriate for beams, columns and walls[42]. The modified Takeda hysteresis model[55] is used for beams (fat) and columns (thin). Beam-column joints are modelled through elastic springs. A more detailed description of both member characterisation and modelling strategy, including illustrations, is given in ref. [56].

A set of 150 natural (i.e., recorded) ground motions is selected from the SIMBAD database, "selected input motions for displacement-based assessment and design"[57]. As per ref. [42], the 3-component 467 records in the database are ranked according to their peak ground acceleration, PGA, values (by using the geometric mean of the two horizontal components) and then keeping the horizontal component with the largest PGA value. The first 150 records are arbitrarily selected, characterised by moment magnitudes in the range [5–7.3], a station-to-source distance smaller than 35 km, and PGA ranging between 0.29g and 1.77g. Such a ground-motion selection approach is consistent with the adopted response analysis method, which is a cloud-based NLTHA[58]. For each ground motion, the frame/wall displacement profiles recorded in the analysis are post-processed to compute the peak effective height displacement (used as an EDP), and the spectral acceleration at the fundamental period is adopted as an IM. Moreover, each ground motion is associated to a binary variable indicating collapse, herein defined as a global dynamic instability (i.e., non-convergence) of the numerical analysis, likely

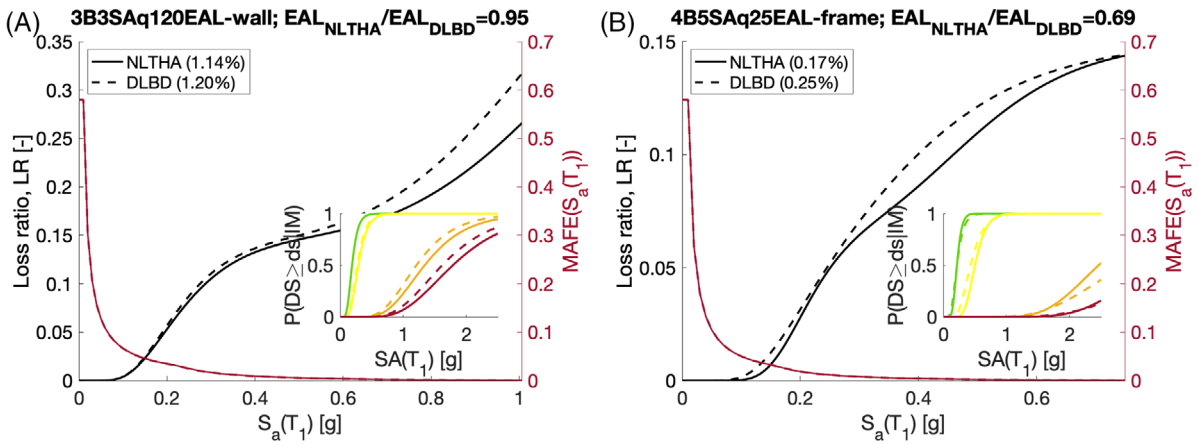

FIGURE 7 Simplified DLBD-based versus refined NLTHA-based losses comparison: (A) best case study, (B) worst case study. MAFE, mean annual frequency of exceedance.

corresponding to a plastic mechanism (i.e., the structure is under-determined) or exceeding the nominal threshold of 10% maximum inter-storey drift.

After deriving the conditional mean and standard deviation of EDP given IM, a PSDM for each frame and wall configuration is defined as the power-law model $EDP = p_1 IM^{p_2}$,[58] in turn obtained via the least square method (p_1 and p_2 are the parameters of the regression). This allows deriving fragility curves compatible with those in Equation (2), where $\eta_{DSi} = \exp(\frac{\ln(\frac{\Delta_{DSi}}{p_1})}{p_2})$ and $\beta = \frac{\sigma}{p_2}$. Collapse cases (roughly 3% of the ground motions) are included in the fragility characterisation according to the procedure in ref. [59], which is described in detail in ref. [42].

4.3 | Discussion on loss estimates

Figure 7 shows a summary plot comparing the refined and simplified loss assessments for the case-study lateral resisting systems providing the best and worst loss discrepancy with respect to the target EAL. All loss comparisons are reported considering the target EAL as a reference for the design, for example, $(EAL_{NLTHA} - EAL_{target})/EAL_{target}$, although the NLTHA-based estimation is considered as a benchmark. The best case study is the wall system within the 3B3SAq120EAL building, showing a relative loss underestimation equal to 5.0%. The worst-performing case study is the frame system within the 4B5SAq25EAL building, showing a loss underestimation equal to 32.0%.

The hazard curves adopted for the refined and simplified loss assessment are essentially superimposed, thus confirming that the period-estimation errors (Section 4.1) are acceptable. The MDoF NLTHA-based vulnerability functions consistently show lower values with respect to those obtained within DLBD, with the error levels increasing as the IM increases. This result is mainly caused by the underestimated DLBD-based fragility medians with respect to the NLTHA ones. As discussed in detail (for eight RC case studies) by Gentile and Galasso[28], this is in turn caused by a combination of: (1) an error on the slope of the PSDM, causing greater errors for more-severe DSs; (2) higher discrepancies on the thresholds of more-severe DSs. Overall, the effect of such errors on the loss estimation is acceptable, especially due to the lower impact of errors at high IM values. It is worth noting that the surrogated PSDM for all the case studies did not involve any IM-wise extrapolation (i.e., the maximum IM in the training dataset of the surrogate PSDM is higher than the maximum IM defined in the hazard curves).

Any discrepancy between loss estimates based on the refined NLTHA-based methodology and the simplified DLBD values not only depends on the adopted response analysis method and related estimation of the PSDM but is also affected by the mismatch between the pushover-based force-displacement curve and the design SDoF one used within DLBD. In turn, such discrepancy involves the elastic period and the DS thresholds, which produce further error propagations. In an attempt to isolate the loss error caused by the PSDM derivation, the simplified loss assessment is repeated after defining the above parameters based on the numerical pushover. This simulates an ideal structural detailing process providing

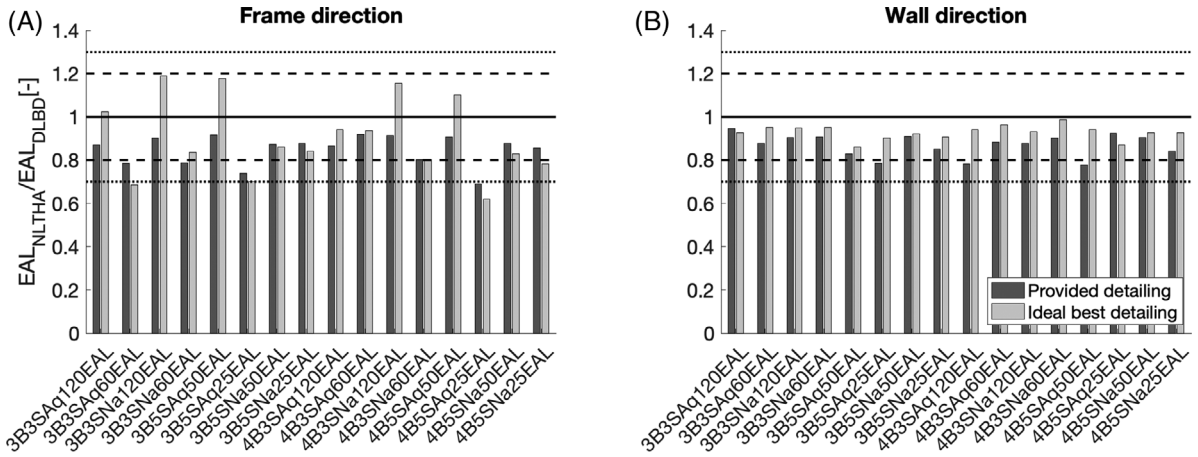

FIGURE 8 Ratio of NLTHA-based EAL versus the simplified DLBD-based one: (A) frame direction; (B) wall direction. The "ideal best detailing" cases are obtained by re-running the simplified loss assessment explicitly using the numerical pushover curves.

an "ideal best detailing", in which the numerical pushover perfectly matches the capacity curve of the design SDoF (as opposed to regular situations involving some level of overdesign in strength and/or ductility capacity).

Figure 8 compares the NLTHA-based loss estimates with the EAL targets in DLBD, both for the frame and wall case studies. For the frame case studies, the NLTHA show a relative loss discrepancy within the range [−30.1% −8.2%], with the median discrepancy being equal to −12.7% and the standard deviation equal to 9.6%. It is worth noting that all the NLTHA predictions confirm that the provided designs are conservative (i.e., loss estimates are lower than the EAL target) and that most of them are below the arguably-acceptable 20% error threshold (in particular, 14 over 16 frame case studies show a discrepancy smaller than 21%).

The results for the wall case studies are overall similar, with a relative loss discrepancy within the range [−22.2% −5.3%], median discrepancy equal to −12.0%, and standard deviation equal to 5.2%. The main difference with the frame case studies is the reduced standard deviation of the errors. On the one hand, this can be attributed to the simplicity of the wall lateral resisting system, which shows a dynamic behaviour closer to an SDoF if compared to a frame system. On the other hand, the above comparison should take into account the definition of the DS thresholds, which depend on a single member typology only (i.e., the wall), compared to the multiple beams and columns defining the frame systems.

The final aspect to discuss refers to over-design, in turn led by conservativism. In fact, it is reasonable to assume that a user of DLBD would provide a structural detailing leading to a force-displacement curve slightly out-performing the design SDoF. Figure 8 allows analysing each case study in its ideal best detailing, thus artificially removing any level of conservativism. Notably, the effects of conservativism are much higher for the frame case studies while practically negligible for walls. This reflects the comparative simplicity of structural detailing for wall systems, for which it is possible to provide designs with a reasonably low over-design (Figure 6B), while this is generally not possible for frames (Figure 6A). The main difference between the two groups of case studies is the standard deviation of the EAL discrepancies, which shifts from 9.6% to 17.9% for frames, while it is almost unchanged for walls (from 5.2% to 3.6%). Moreover, the NLTHA of five frame case studies show exceeds the target EAL, thus indicating cases of non-conservative loss estimations. As mentioned above, the EAL discrepancies of the ideal best detailing case studies should be ascribed only to errors in the estimation of the probabilistic seismic demand model. In turn, this refers to the MDoF versus SDoF differences, which are larger for frames than for walls. This specific discussion allows one to appraise how conservativism in detailing, which is likely to be present in most design cases, can effectively counterbalance some of the inherent inaccuracies of the present DLBD procedure and lead to a reasonable conservativism in the loss estimates (especially considering the simplicity of DLBD).

5 | CONCLUSION

This paper proposed a direct loss-based design (DLBD) procedure for RC frame and wall lateral resisting systems. DLBD aims at designing structures that would achieve, rather than be bounded by, a given loss-related metric under the relevant

site-specific seismic hazard (by analogy with the words of Priestley[8]). The adjective "direct" refers to the ability of the designer to specify a target loss as an input parameter before running any analysis, and to achieve such a target virtually without design iterations (e.g., one to three are usually sufficient). DLBD originates from the initial procedure proposed by Gentile and Galasso[28]. The procedure is based on a flexible and fast mapping returning the force-displacement curve of candidate design SDoF systems complying with the desired target loss. By linking a target loss to a target capacity curve using a simple approach, DLBD allows designers to target such loss by matching a structural details configuration to such force–displacement curve. The code to apply the proposed procedure is freely available in an online repository (https://github.com/robgen/lossBasedDesign).

The proposed DLBD is demonstrated for 16 reinforced concrete, rectangular-plan buildings composed of frames in their longitudinal direction and walls in the transverse one (thus considering 32 case-study lateral resisting systems). Each case study is analysed via a more-refined earthquake loss assessment methodology based on non-linear time-history analyses (NLTHA) of component-by-component multi degree of freedom models, and the results are compared to the selected target losses. All the NLTHA predictions confirm that the provided designs are conservative (i.e., loss estimates are lower than the target loss), and most of them are below the 20% error threshold. In particular, the relative discrepancy $(EAL_{NLTHA} - EAL_{target})/EAL_{target}$ is *within 10% for 12 out of 32 case studies, between 10% and 20% for 13, between 20% and 31% for the remaining six.*

Although the results are promising, a final verification against more refined, component-by-component methodologies for loss analysis (e.g., FEMA P58, as opposed to the adopted building-level approach) is needed to confirmgit the confidence with which DLBD allows to set a target loss level. The refined component-by-component loss estimations should also include the effect of epistemic uncertainties to verify if the simplified DLBD loss predictions lie within the epistemic uncertainty bounds. Such validation exercises could be potentially used to provide correction factors to the simplified loss estimates at the basis of the proposed DLBD.

The proposed DLBD shows high potential in assisting the conceptual phase of the design process by allowing the designer to rationally consider different design options (e.g., different materials and lateral resisting systems) and discriminate among them on the basis of the target loss. In this paper, this is demonstrated for a simple example in which DLBD is used to select the most feasible option between a frame and a wall lateral resisting system for buildings of different heights. Provided that the DLBD procedure is specialised for more design cases, the conceptual design approach shown here could be applied considering different materials (e.g., timber, pre-cast concrete, steel) and lateral resisting systems (e.g., dual wall-frame systems, braced frames, rocking structures, base-isolated structures). Further research is suggested to extend the scope of DLBD, especially considering that any design use case (e.g., structure type, material, lateral resisting system) for which a direct displacement-based design is available can be "upgraded" to DLBD by following the conceptual framework of this paper.

ACKNOWLEDGEMENTS

This study was partially funded by the European Union's Horizon 2020 research and innovation program under grant agreement No. 843794 (Marie Sk1odowska-Curie Research Grants Scheme MSCA-IF-2018: Multi-level Framework to Enhance Seismic Resilience of RC buildings—MULTIRES).

DATA AVAILABILITY STATEMENT

The data that support the findings of this study are openly available in the repository "robgen—lossBasedDesign" at https://github.com/robgen/lossBasedDesign

ORCID

Roberto Gentile https://orcid.org/0000-0002-7682-4490

REFERENCES

1. Iervolino I, Spillatura A, Bazzurro P. Seismic reliability of code-conforming Italian buildings. *J Earthq Eng*. 2018;22:5-27. doi:10.1080/13632469.2018.1540372
2. SEAOC Vision 2000 Committee. *Performance-Based Seismic Engineering. Structural Engineers Association of California*. SEAOC Vision 2000 Committee; 1995.
3. Cornell CA, Krawinkler H. Progress and challenges in seismic performance assessment. *PEER Center News*. 2000;3(2):1-2.
4. D'Ayala D, Meslem A, Vamvatsikos D, et al. Guidelines for analytical vulnerability assessment - low/mid-rise. *GEM Technical Report*; 2013. doi:10.13117/GEM.VULN-MOD.TR2014.12

5. Federal Emergency Management Agency. Seismic performance assessment of buildings. *Volume 1–Methodology*; 2012.
6. Almuftti I, Willford MR. Resilience-based Earthquake Design Initiative (REDi) for the next generation of buildings. *ARUP Report*; 2013.
7. European Committee for Standardisation (CEN). *EN 1998-1. Eurocode 8: Design of structures for earthquake resistance. Part 1: General rules, Seismic action and rules for buildings*. European Committee for Standardisation (CEN); 2005.
8. Priestley MJN, Calvi GM, Kowalsky MJ. *Displacement-based seismic design of structures*. IUSS Press; 2007.
9. Aschheim M, Black EF. yield point spectra for seismic design and rehabilitation. *Earthq Spectra*. 2000;16(2):317-335. doi:10.1193/1.1586115
10. Long XH, Fan J, Nie FF, Zhang YT. Seismic fragility based optimum design of LRB for isolated continuous girder bridge. *Int J Struct Civ Eng Res*. 2015; 4(3):231–236. doi:10.18178/ijscer.4.3.231-236
11. Aljawhari K, Gentile R, Galasso C. A fragility-oriented approach for seismic retrofit design. *Earthq Spectra*. 2022;38(3):1813-1843. doi:10.1177/87552930221078324
12. Vamvatsikos D, Aschheim MA. Performance-based seismic design via yield frequency spectra ‡. *Earthq Eng Struct Dyn*. 2016;45(11):1759-1778. doi:10.1002/eqe.2727
13. Franchin P, Pinto PE. Method for probabilistic displacement-based design of RC structures. *J Struct Eng*. 2012;138(5):585-591. doi:10.1061/(ASCE)ST.1943-541X.0000492
14. Franchin P, Petrini F, Mollaioli F. Improved risk-targeted performance-based seismic design of reinforced concrete frame structures. *Earthq Eng Struct Dyn*. 2018;47(1):49-67. doi:10.1002/eqe.2936
15. Žižmond J, Dolšek M. Formulation of risk-targeted seismic action for the force-based seismic design of structures. *Earthq Eng Struct Dyn*. 2019;48(12):1406-1428. doi:10.1002/eqe.3206
16. Hu S, Chen B, Song G, Wang L. Resilience-based seismic design optimization of highway RC bridges by response surface method and improved non-dominated sorting genetic algorithm. *Bull Earthq Eng*. 2022;20(1):449-476. doi:10.1007/s10518-021-01232-8
17. Vamvatsikos D, Kazantzi AK, Aschheim MA. Performance-based seismic design: Avant-Garde and code-compatible approaches. *ASCE-ASME J Risk Uncertainty Eng Syst, A: Civ Eng*. 2016;2(2):C4015008. doi:10.1061/AJRUA6.0000853
18. Aschheim M, Hernández-Montes E, Vamvatsikos D. *Design of Reinforced Concrete Buildings for Seismic Performance*. Boca Raton : Taylor & Francis, a CRC Title, Part of the Taylor & Francis Imprint, a Member of the Taylor & Francis Group, the Academic Division of T& F Informa, Plc, [2019]. CRC Press; 2019. doi:10.1201/b19964
19. Gentile R, Galasso C. Simplicity versus accuracy trade-off in estimating seismic fragility of existing reinforced concrete buildings. *Soil Dyn Earthq Eng*. 2021;144:106678. doi:10.1016/j.soildyn.2021.106678
20. Dhakal RP, Saha SK. Loss optimization seismic design (losd): beyond seismic loss assessment. *16th World Conference on Earthquake Engineering, Santiago, Chile*; 2017.
21. Mackie KR, Stojadinović B. Performance-based seismic bridge design for damage and loss limit states. *Earthq Eng Struct Dyn*. 2007;36(13):1953-1971. doi:10.1002/eqe.699
22. Pei S, van de Lindt JW. Systematic seismic design for manageable loss in wood-framed buildings. *Earthq Spectra*. 2009;25(4):851-868. doi:10.1193/1.3240412
23. Shahnazaryan D, O'Reilly GJ. Integrating expected loss and collapse risk in performance-based seismic design of structures. *Bull Earthq Eng*. 2021;19(2):987-1025. doi:10.1007/s10518-020-01003-x
24. Krawinkler H, Zareian F, Medina RA, Ibarra LF. Decision support for conceptual performance-based design. *Earthq Eng Struct Dyn*. 2006;35(1):115-133. doi:10.1002/eqe.536
25. Sinković NL, Brozovič M, Dolšek M. Risk-based seismic design for collapse safety. *Earthq Eng Struct Dyn*. 2016;45(9):1451-1471. doi:10.1002/eqe.2717
26. Esmaili O, Zareian F. Preliminary design of moment-resisting frame buildings for tolerable financial loss. *J Struct Eng*. 2019;145(7):04019059. doi:10.1061/(ASCE)ST.1943-541X.0002331
27. Takahashi N, Shiorara H, Nakano Y. Equivalent seismic loss spectrum for a performance based design of sustainable r/c buildings. *8th U.S. National Conference on Earthquake Engineering, San Francisco, California, USA*; 2006.
28. Gentile R, Galasso C. Surrogate probabilistic seismic demand modelling of inelastic single-degree-of-freedom systems for efficient earthquake risk applications. *Earthq Eng Struct Dyn*. 2022;51(2):492-511. doi:10.1002/eqe.3576
29. Calvi GM, O'Reilly GJ, Andreotti G. Towards a practical loss-based design approach and procedure. *Earthq Eng Struct Dyn*. 2021;50(14):3741-3753. doi:10.1002/eqe.3530
30. Stucchi M, Meletti C, Montaldo V, Crowley H, Calvi GM, Boschi E. *Seismic hazard assessment (2003-2009) for the Italian building code*. Bulletin of the Seismological Society of America; 2011. doi:10.1785/0120100130
31. Peruš I, Klinc R, Dolenc M, Dolšek M. Innovative Computing Environment for Fast and Accurate Prediction of Approximate IDA Curves; 2013. doi:10.1007/978-94-007-6573-3_13
32. Minas S, Galasso C. Accounting for spectral shape in simplified fragility analysis of case-study reinforced concrete frames. *Soil Dyn Earthq Eng*. 2019;119:91-103. doi:10.1016/j.soildyn.2018.12.025
33. Rasmussen CE, Williams CKI. *Gaussian Processes for Machine Learning*. The MIT Press; 2006.
34. Ghosh J, Padgett JE, Dueñas-Osorio L. Surrogate modeling and failure surface visualization for efficient seismic vulnerability assessment of highway bridges. *Prob Eng Mech*. 2013;34:189-199. doi:10.1016/j.probengmech.2013.09.003
35. Kircher CA, Whitman RV, Holmes WT. HAZUS earthquake loss estimation methods. *Nat Hazard Rev*. 2006;7(2):45-59. doi:10.1061/(asce)1527-6988(2006)7:2(45)

36. European Committee for Standardisation (CEN). Eurocode 8: Design of structures for earthquake resistance. Part 3: Strengthening and repair of buildings; 2005.
37. New Zealand Society for Earthquake Engineering (NZSEE). *The seismic assessment of existing buildings - technical guidelines for engineering assessments*. New Zealand Society for Earthquake Engineering (NZSEE); 2017.
38. Ramirez CM, Miranda E. *Building-Specific Loss Estimation Methods & Tools for Simplified Performance-Based Earthquake Engineering. Report No 171*; 2009.
39. Papadopoulos AN, Vamvatsikos D, Kazantzi AK. Development and application of FEMA P-58 compatible story loss functions. *Earthq Spectra*. 2019;35(1):95-112. doi:10.1193/102417EQS222M
40. Shahnazaryan D, O'Reilly GJ, Monteiro R. Story loss functions for seismic design and assessment: development of tools and application. *Earthq Spectra*. 2021;37(4):2813-2839. doi:10.1177/87552930211023523
41. Gentile R, Pampanin S, Galasso C. A computational framework for selecting the optimal combination of seismic retrofit and insurance coverage. *Comput-Aided Civ Infrastruct Eng*. 2021;37(8):956-975. doi:10.1111/mice.12778. in press.
42. Gentile R, Galasso C. Gaussian process regression for seismic fragility assessment of building portfolios. *Struct Saf*. 2020;87:101980. doi:10.1016/j.strusafe.2020.101980
43. Project Management Institute. *A Guide to the project management body of knowledge*. Project Management Institute; 2013. doi:10.5860/choice.34-1636
44. O'Reilly GJ, Calvi GM. Conceptual seismic design in performance-based earthquake engineering. *Earthq Eng Struct Dyn*. 2019;48(4):389-411. doi:10.1002/eqe.3141
45. Cosenza E, del Vecchio C, di Ludovico M, et al. *The Italian guidelines for seismic risk classification of constructions: technical principles and validation*. Springer; 2018. doi:10.1007/s10518-018-0431-8
46. Freeman SA. Review of the development of the capacity spectrum method. *ISET J Earthq Technol*. 2004;41(1):1-13.
47. Dolšek M, Lazar Sinković N, Žižmond J. IM-based and EDP-based decision models for the verification of the seismic collapse safety of buildings. *Earthq Eng Struct Dyn*. 2017;46(15):2665-2682. doi:10.1002/eqe.2923
48. Nettis A, Gentile R, Raffaele D, Uva G, Galasso C. Cloud capacity spectrum method: accounting for record-to-record variability in fragility analysis using nonlinear static procedures. *Soil Dyn Earthq Eng*. 2021;150:106829. doi:10.1016/j.soildyn.2021.106829
49. Suarez D, Rubini G, Gentile R, Galasso C. Gaussian process regression-based surrogate modelling for direct loss-based seismic design of low-rise base-isolated structures. XIX Convegno Nazionale Associazione Nazionale Italiana di Ingegneria Sismica (ANIDIS) – L'Ingegneria Sismica in Italia; 2022.
50. Consiglio dei Ministri. DM 17 gennaio 2018 in materia di "aggiornamento delle norme tecniche per le costruzioni". Gazzetta ufficiale n.42 del 20 febbraio 2018; 2018.
51. Gentile R. SLaMA Solver Frame - Graphical user interface software for the Simple Lateral Mechanism Analysis (SLaMA). Practical and theoretical manual (https://www.robertogentile.org/en/SLaMAf, last access: 01/07/2023); 2019.
52. Gentile R, Pampanin S, Raffaele D, Uva G. Non-linear analysis of RC masonry-infilled frames using the SLaMA method: part 1—mechanical interpretation of the infill/frame interaction and formulation of the procedure [Open Access]. *Bull Earthq Eng*. 2019;17(6):3283-3304. doi:10.1007/s10518-019-00580-w
53. Carr AJ. *RUAUMOKO2D – The Maori God of Volcanoes and Earthquakes. Inelastic Analysis Finite Element program*; 2016.
54. Magenes G, Pampanin S. Seismic response of gravity-load design frames with masonry infills. *13th World Conference on Earthquake Engineering*; 2004.
55. Saiidi M, Sozen M. *Simple and complex models for nonlinear seismic response of reinforced concrete structures*; 1979.
56. Gentile R, Pampanin S, Raffaele D, Uva G. Analytical seismic assessment of RC dual wall/frame systems using SLaMA: proposal and validation. *Eng Struct*. 2019;188:493-505. doi:10.1016/j.engstruct.2019.03.029
57. Smerzini C, Galasso C, Iervolino I, Paolucci R. Ground motion record selection based on broadband spectral compatibility. *Earthq Spectra*. 2014;30(4):1427-1448. doi:10.1193/052312EQS197M
58. Jalayer F, Cornell CA. Alternative non-linear demand estimation methods for probability-based seismic assessments. *Earthq Eng Struct Dyn*. 2009;38(8):951-972. doi:10.1002/eqe.876
59. Jalayer F, Ebrahimian H, Miano A, Manfredi G, Sezen H. Analytical fragility assessment using unscaled ground motion records. *Earthq Eng Struct Dyn*. 2017;46(15):2639-2663. doi:10.1002/eqe.2922

How to cite this article: Gentile R, Calvi GM. Direct loss-based seismic design of reinforced concrete frame and wall structures. *Earthquake Engng Struct Dyn*. 2023;1-21. https://doi.org/10.1002/eqe.3955